

Implicit Large Eddy Simulation of a wingtip vortex at $Re_c = 1.2 \cdot 10^6$

Jean-Eloi W. Lombard^{*}, David Moxey[†], Julien F. A. Hoessler[‡],
Sridar Dhandapani[§], Mark J. Taylor[¶], Spencer J. Sherwin^{||}

Abstract

In this article we present recent developments in numerical methods for performing a Large Eddy Simulation (LES) of the formation and evolution of a wingtip vortex. The development of these vortices in the near wake, in combination with the large Reynolds numbers present in these cases, make these types of test cases particularly challenging to investigate numerically. We first give an overview of the Spectral Vanishing Viscosity-implicit LES (SVV-iLES) solver that is used to perform the simulations, and highlight techniques that have been adopted to solve various numerical issues that arise when studying such cases. To demonstrate the method's viability, we present results from numerical simulations of flow over a NACA 0012 profile wingtip at $Re_c = 1.2 \cdot 10^6$ and compare them against experimental data, which is to date the highest Reynolds number achieved for a LES that has been correlated with experiments for this test case. Our model correlates favorably with experiment, both for the characteristic jetting in the primary vortex and pressure distribution on the wing surface. The proposed method is of general interest for the modeling of transitioning vortex dominated flows over complex geometries.

Nomenclature

| | | | | | |
|------------|---|--|---------------------|---|---|
| c | = | Wing chord | τ | = | Kolmogorov time scale |
| b | = | wingspan | p | = | pressure |
| A | = | aspect ratio of the wing | p | = | far-field pressure |
| Re_c | = | Reynolds number based on wing chord | U_∞ | = | inflow velocity |
| x, y, z | = | Cartesian coordinates, | ρ_∞ | = | density |
| Δx | = | local cell size | C_p | = | Pressure coefficient |
| u, v, w | = | Cartesian velocity components | ν | = | kinematic viscosity |
| y^+ | = | distance from surface in wall units | α | = | angle of attack |
| t | = | time | k | = | mode |
| t_c | = | convective time associate to chord | M | = | cut-off mode of the SVV filter |
| Δt | = | time-step | P | = | $P = M - 1$ polynomial order of the spectral element. |
| l_0 | = | length scale associate to largest eddies | ε_{SVV} | = | diffusion from the SVV filter |
| η | = | Kolmogorov length scale | \hat{Q} | = | SVV kernel |

1 Introduction

Understanding the development and growth of wingtip vortices over lifting surfaces is an ongoing research topic both in academia and industry. From an academic perspective, fundamental open questions remain, such as

^{*}Graduate Research Assistant, Department of Aeronautics, Imperial College, London, UK;
jean-eloi.lombard12@imperial.ac.uk (Corresponding Author).

[†]Research Associate, Aeronautics, Department of Aeronautics, Imperial College, London, UK

[‡]Senior CFD Engineer, CFD Technology, McLaren Racing, McLaren Technology Center, Woking, UK

[§]Team Leader, CFD Technology, McLaren Racing, McLaren Technology Center, Woking, UK

[¶]Principle Aerodynamicist, McLaren Racing, McLaren Technology Center, Woking, UK

^{||}Professor of Computational Fluid Mechanics, Aeronautics.

the possible re-laminarization of the vortex as it is shed from the wing [1] and the origin of meandering [2, 3, 4], the low-frequency movement of the vortex core and the evolution of the vortex structure. Vortices shed from lifting surfaces pose challenges to model in many an industrial context such as wind turbines, helicopter blades, high-lift configuration of aircraft and high-performance automotive industry [5, 6, 7, 8, 9]. Developing a better understanding of the near-wake of the vortex, lying within one chord length of the trailing edge of the lifting surface, is therefore essential in understanding the complex flow-structure interactions of interest in these problems. The far-field properties of these vortices are also a challenge for the aeronautics industry, where their persistence imposes strict limits on distances between landing aircraft [10]. For these reasons we are interested in refining modeling methods for investigating the growth of the vortex in the near-field.

Conceptually, the simplest approach to ensure that the flow physics are accurately simulated is to perform a direct numerical simulation (DNS), in which all necessary scales are resolved at a given Reynolds number. For cases at even moderately high Re however, this approach is clearly unfeasible. To demonstrate this, let us assume the Kolmogorov hypothesis holds for this flow and as a very rough approximation that the length scale l_0 associated to the largest eddies is of the same order as the chord length $l_0 \approx c$. The number of grid points needed to resolve the Kolmogorov length-scale relates with the Reynolds number as $\eta \sim Re^{-3/4}$, meaning that three-dimensional simulation of a uniformly turbulent flow requires a resolution of $Re^{9/4}$ grid points. For aeronautical test cases, where Re is typically $O(10^6)$ or $O(10^7)$, we therefore require $O(10^{14})$ to $O(10^{16})$ grid points to resolve the flow. Even accounting for variations in geometry which may permit varying resolution throughout the domain, based on the current rate of advancement of high-performance computing (HPC) facilities, resolving fully developed three-dimensional flow at high Reynolds number in a timely manner will continue to be well out of reach for the foreseeable future.

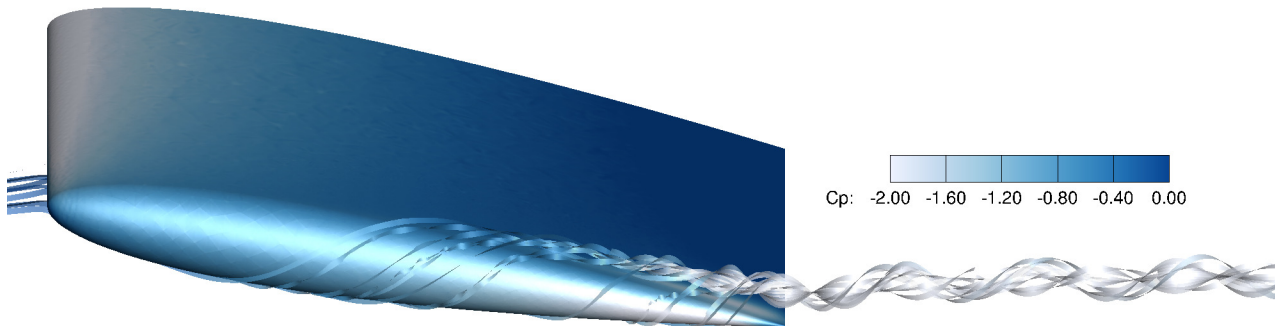


Figure 1: Wingtip vortex developing over a NACA 0012 profile with rounded wing cap in a wind tunnel, modeling the experimental setup of Chow *et al.*[1] Both wing surface and streamlines are colored by static pressure coefficient $C_p = 2 \cdot (p - p_\infty) / \rho_\infty U_\infty^2$ where $U_\infty^2 = 1$ and $\rho_\infty = 1$.

Consequently, there has been ongoing development of modeling methods where small turbulent scales are not explicitly computed. Traditional Reynolds Averaged Navier Stokes (RANS) methods, alongside more recent advanced such as the Reynolds Stress methods [11], have been developed to simulate both the complex three-dimensional transitioning boundary layer on the wing and the highly curved flow within the vortex. More computationally-intensive methods, such as LES and Lattice Boltzmann VLES[12] have also been developed or adapted to investigate such flows, in correlating the simulated results to experimental data. The lattice Boltzmann method has been used in conjunction with a modified $k - \varepsilon$ two-equation turbulence model as well as turbulence wall shear stress model were used to perform a VLES where the walls were the turbulent flow at the wall was modelled.

The key feature of these studies is in their use of reduced equations or turbulence models, all of which require parameters to tune their performance. Since the underlying physical processes that dictate the development and evolution of vortices is not well understood, it is therefore difficult *a priori* to determine appropriate settings for these models. The aim of this work is therefore to demonstrate how an implicit LES method, in which the number of parameters is comparably very small and is used to provide additional stability, can successfully be leveraged to obtain accurate comparisons against experimental data. We appreciate that there may be different views of the definition of implicit LES. We have adopted the definition of Sagaut [13], who explicitly refers to SVV as an implicit LES model and states that “*using a numerical viscosity with no*

explicit modeling are all based implicitly on the hypothesis [...] the action of subgrid scales on the resolved scales is equivalent to a strictly dissipative action.” The only influence of the sub-grid scales on the resolved scales is therefore dissipative.

Many existing LES codes are based on finite volume, linear finite element or Cartesian grid methods. We will instead investigate the viability of the spectral/*hp* element method, which lies in the class of high-order finite element methods. These methods are widely used in academia, as they offer attractive properties such as exponential convergence and low dissipation error for sufficiently smooth solutions [14]. This is significant, as faithfully modeling the wingtip vortex in the far wake is of particular interest in many research communities and industries. It is implied that accurate modelling of the far field vortex requires precise modelling of the vortex onset in the near field using high precision, low dissipation schemes [15, 16, 1, 17, 18]. However, these methods have not been widely applied for the type of industrial, high-*Re* cases that we consider in this work. Such methods are generally perceived as difficult to implement, as a range of specialised preconditioners, mesh generation procedures, parallel communication strategies and stabilisation approaches are needed to successfully complete a simulation.

In this paper we present the SVV-iLES formulation, which utilises the spectral vanishing viscosity approach to stabilise numerics [19]. We show how the issues of implementation and mesh generation can be overcome, as well as highlight the benefits that these schemes can have for industrial problems, both in terms of resolution power relative to existing studies and computational efficiency. To demonstrate the viability and robustness of the scheme, we consider the test case presented by Chow *et al.* [1], in which the flow over a NACA 0012 wingtip has been investigated with precise experimental measurements. This case has subsequently become a benchmark for vortex dominated flows. To this end we perform an SVV-iLES, at the highest Reynolds number considered so far for this case, and correlate our results to the experimental data. As in previous numerical studies, in order to reduce the computational cost we have chosen to run the computation at a lower Reynolds number. In this work we set $Re = 1.2 \cdot 10^6$, as compared to the experiment which uses $Re = 4.6 \cdot 10^6$.

In the following section we will briefly report the experimental and numerical methods that have been developed and evaluated for investigating the nascent wingtip vortex, as well as the key findings of these studies. We then discuss the key features of the SVV-iLES method in Section 3 and the numerical methodology for our simulations. The evaluation of the SVV-iLES, by close comparison with the extensive data from the experiment of Chow *et al.*[1] and numerical results of Uzun *et al.*[5], is presented in Section 4 before we conclude in Section 5 with a brief overview of the key findings.

2 Literature review

We begin with a brief presentation of existing work in the investigation of wingtip vortices; other thorough reviews of this field can be found in Rossow [7], Spalart [10] and Green & Acosta [20]. Firstly, experimental studies are considered and a summary of the types of flow dynamics that exists for these cases is presented. We then discuss results obtained by numerical simulations before emphasizing the possible drawbacks of an explicit subgrid-scale model in the context of complex flows, such as the wingtip vortex and highlight the originality of the method employed in this study.

2.0.1 Experimental methods

For the wingtip vortex the Reynolds number is computed from the chord length c as $Re_c = cU_\infty/\nu$, where U_∞ is the free stream velocity and ν is the kinematic viscosity. Giuni [21, 22] and Giuni & Benard [23] investigated the initial formation and development of the wingtip vortex on a NACA 0012 rectangular wing with both square and rounded wingtips at $Re_c = 7.4 \cdot 10^5$ for angles of attack $\alpha = 0^\circ, 4^\circ$ and 12° . They reported that for a given fixed angle of attack, a ‘more’ axisymmetric vortex sheds from the rounded wingtip with stronger vorticity within its core compared the square-tip wing. They also reported that for the $\alpha = 12^\circ$ case the axial velocity excess is higher for the rounded wingtip. This region is surrounded by a region of axial velocity deficit corresponding to rolling up of the vorticity sheet. The weaker axial velocity excess for the square wingtip is believed to be a consequence of the more numerous secondary vortices generated by the square wingtip.

Defining the center of the primary vortex as the location of the streamwise helicity peak, they investigated the meandering of the vortex in the near field. Two distinct modes of behaviour were observed: for the

squared wingtip, the meandering decreased with the distance from the trailing edge whereas for the rounded wingtip case, the meandering grew quasi-linearly with distance from the trailing edge. This has also been reported by Devenport *et al.* [2] and Giuni *et al.* [22]. However Jacquin *et al.* [3] concluded vortex meandering to be insensitive to free stream unsteadiness in the wind tunnel. Fabre & Jacquin [24, 25] and Dieterle *et al.* [26] suggested meandering might also be influenced by the destabilization of a vortex by secondary vortex of opposite sense. Jacquin goes further by reporting that the various co-operative interactions between primary and secondary vortices affected the same range of frequencies as meandering. Zuhail [27] and Zuhail & Gahrib [28] investigated the correlation between number and strength of secondary vortices and the amplitude of meandering. McAlister [29] investigated the wingtip vortex of NACA 0015 with both rounded and square wing cap reporting the maximum azimuthal velocity of the vortex to be independent of Reynolds number but dependent on the angle of attack.

Finally, Chow *et al.* [1] performed an extensive experimental and numerical study of the wingtip vortex over a rounded NACA 0012 profile in view of defining a benchmark for numerical models. They reported merging of the secondary and tertiary vortices into the primary within one chord length of the trailing edge. From this distance onwards, the vortex had an axisymmetric structure with a jet-like axial velocity profile (i.e. the axial velocity within the vortex core was greater than the freestream velocity). The peak jetting velocity was measured to be $1.77U_\infty$ at the trailing edge and by three-quarters of a chord length downstream of the trailing edge it was measured to be $1.7U_\infty$. Pressure taps were placed on the wing-surface to assess the state of the boundary layer, both under the primary vortex where a strong suction region is present and at different spanwise locations, allowing for insight into the three dimensional boundary layer. They also reported skin-friction lines to gain understanding into the attachment and detachment lines of the strongest vortices in the near wake, as well as low amplitudes of meandering because of both a relatively large angle of attack of $\alpha = 10^\circ$ and measurements at relatively short distances from the trailing edge. Devenport *et al.* [2] reported meandering amplitude growing linearly with distance from trailing edge.

2.0.2 Numerical methods

Presently, RANS based methods with linear eddy viscosity models, such as $k - \omega$ SST and $k - \epsilon$, remain commonplace for industrial flow simulation [11]. For vortex dominated flows, and more generally flows with strong curvature, these models may struggle due to the largely unsteady dynamics of the flow. Large discrepancy with experimental data, exceeding 100% error on C_p distribution in the vortex core, as well as drastic under-prediction of the jetting within the core have been reported by Churchfield *et al.* [30]. These results have motivated the development, over the past 30 years, of more complex closure models tailored for highly curved flows such as the wingtip vortex. We present a brief overview of this development.

Dacles-Mariani *et al.* [9] ran a 5th order compact (i.e. 7 point stencil instead of 11) biased upwind scheme for the advection term and second order scheme for the viscous term. Here they underline the necessity for low numerical dissipation. They ran a modified version of the one-equation Baldwin-Barth turbulence model where they modified the production term to avoid overproduction of eddy viscosity in the vortex core. They successfully captured a secondary structure and computed the axial velocity profiles of the core to within 3% of experiment but under-predicted the core pressure by more than 25%. It should also be stressed that Dacles-Mariani *et al.* [31] used experimental data to setup both inflow and outflow boundary conditions for their RANS simulation. Linear eddy-viscosity being too dissipative, Craft *et al.* [32] developed a non-linear eddy viscosity model (EVM). This more advanced model still suffered from a more severe decay of the turbulent stresses than measured experimentally. Duraisamy and Iaccarino [33] modified the eddy viscosity coefficient of the $v^2 - f$ turbulence model and compared their results favorably for axial surplus compared to the baseline Spallart-Allmaras and Menter's $k - \omega$ SST models. The wingtip vortex exhibits a peculiarity in the turbulence structures where the stress and strain are out of phase which renders questionable the use isotropic eddy-viscosity based prediction methods such as ($k-\omega$, etc). Churchfield *et al.* [34, 35, 15, 11] modified the Spallart-Allmaras model to account for streamline curvature and successfully modeled the lag between the mean strain rate and respective Reynolds stress. This method produced the best correlation with experiment, for a RANS based method, but proved costly (relative to other simpler RANS methods) and so their use may be restricted to flows dominated by vortices. They also showed that without the accurate modeling of the three dimensional boundary layer the developing vortex remained challenging to compute accurately even for the advanced RANS models correcting for the high degree of curvature in the flow.

In an attempt to develop increasingly robust models, more advanced numerical methods such as Large

Eddy Simulation (LES) and Very Large Eddy Simulations (VLES) have been proposed to investigate unsteady features of the flow as well as aero-acoustic properties. Fleigh *et al.* [36] developed a compressible LES to investigate far-field broadband noise generated by the nascent vortex on a rotating wingtip at Reynolds $Re_c = 1 \cdot 10^6$ and reported computed power and thrust coefficients for the windmill blade within 3% of experimental data. Ghias [8] reported a compressible LES of NACA2415 with square tip run at $Re_c = 10^5$ where they employed a dynamic sub-grid scale model but did not present the correlation of their data with experiment. Uzun *et al.* [5, 6] numerically investigated Chow’s experiment with a compact finite differencing LES with implicit spatial filtering at $Re_c = 5 \cdot 10^5$. Their results were included in the following comparison of our simulations with experimental data. Jiang *et al.* [37] reported results for a LES simulation of Chow’s experiment at the experimental Reynolds number of $Re_c = 4.6 \cdot 10^6$ but did not compare the results with experiment. The lattice Boltzman method was used in conjunction with a modified $k - \varepsilon$ two equation turbulence model and wall shear stress model to perform a VLES. Despite good correlation with the experimental results of Chow *et al.* [1] for the suction of the vortex on the surface of the wing the method over-predicted the jetting phenomena within the vortex by 23% at streamwise location $x/c = -0.114$ and 12% at $x/c = 0.456$. So far these more advanced modeling methods have generally been used for simulations at lower Reynolds numbers [37, 6] or have not not been compared against experimental data in the way they will be in the present study [5].

2.0.3 Motivation and contributions of present study

Modeling unknown physics by leveraging a sub-grid scale model outside of its operational window can be seen as a substantial drawback for explicit sub-grid scale models, which tend to rely on a wide range of parameters to dictate their behaviour. The two-equation eddy-viscosity $k - \omega$ SST turbulence model introduced by Menter [38] in 1994, for example, relies on 9 modeling constants. Menter underlines, in this paper, the strong sensitivity of the resulting computed flow to variations of 5-10% of these constants and further stressing “None of the available theoretical tools (dimensional analysis, asymptotic expansion theory, use of direct numerical simulations (DNS) data, renormalization group (RNG) theory, rapid distortion theory, etc.) can provide constants to that degree of accuracy.” Leveraging these many parameter sub-grid scale models, such as $k - \omega$ SST and more recently Reynolds Stress Relaxation models [11], in complex flow cases therefore requires an *a priori* knowledge of the flow physics. This is often infeasible, particularly when complex geometries are present and the length scales of both flow and geometry vary substantially. For example, in engineering applications such as flow over a Formula 1 car, different sets of parameters may be required to accurately model the various flow dynamics that are induced by the variations in geometry across the body of the the car. This includes the vortex dominated flow of the wing-tip regions of a front wing, regions of the front wing where the flow is mostly two-dimensional, and the rotating wheel that impinges on the moving road. It may therefore be impossible to obtain values for these parameters that capture the desired flow features across the entire car.

The aim of this paper is to show that regularized high order spectral/*hp* element methods, without an explicit sub-grid model, can be applied to produce results that compare favorably against experimental data, by considering flow over a three-dimensional geometry of practical interest. The SVV-iLES approach, which we will present in the following section, requires the choice of two regularization parameters: one to dictate the level of artificial viscosity, and another for a cut-off wavenumber. These are chosen through experimentation, such that the computation does not diverge but do not require assumptions regarding the physics of the flow. We discuss this methodology in the following section before showing results of the NACA 0012 wingtip vortex case.

3 Computational Methodology

In this section, we give a brief summary of the computational methodology used for the NACA 0012 wingtip simulations. We begin by outlining the Nektar++ spectral/*hp* element framework in which the solver is implemented [39]. We then outline the types of regularization that are necessary to perform the computations and prevent the simulation from diverging, along with the mesh generation procedures that are used to generate a curvilinear boundary layer mesh for the geometry. Finally, we discuss initial and boundary conditions as well as resolution requirements in space and time for the simulations.

3.1 Nektar++: a high-order spectral/*hp* element framework

High-order finite element methods often suffer from the stigma of difficulty of implementation, which in turn means that despite their attractive numerical properties and the ability to resolve difficult cases such as the one presented here, they are frequently under-used. Nektar++ is a framework designed to address this problem by providing a modern development environment for these methods. It is highly parallel, providing a range of efficient preconditioners and has support for a variety of solvers including the incompressible Navier-Stokes equations. For a summary of functionality one can see for example Cantwell *et al.* [39], or for more details on the method itself, the reference book by Karniadakis & Sherwin [40].

In the following sections, we outline the modifications made to Nektar++ in order to adapt the existing DNS solver, making it suitable for an iLES approach through regularization. Furthermore we outline the other challenges that need to be addressed in order to more generally make spectral/*hp* element methods viable for these problems.

3.2 From DNS to SVV-iLES: filtering with Spectral Vanishing Viscosity

Running cases at high-Reynolds number on an under-resolved mesh requires close inspection of the source of errors. The highly non-linear nature of the underlying equations leads to a complex interactions of these errors, which when left uncorrected leads to a diverging solution. Broadly, we have found that the two most important aspects are:

1. consistent integration of non-linear terms;
2. artificial dissipation to prevent divergence of the flow in the presence of under-resolution.

We now explain each point in more detail. The incompressible Navier-Stokes solver used in Nektar++ directly integrates the underlying equations through the use of an operator splitting scheme in combination with a consistent boundary condition for the pressure Poisson equation [41]. In this scheme, nonlinear terms are computed explicitly at each quadrature point, which depending on the element type uses a form of Gauss quadrature. These nonlinear terms are then multiplied by the elemental basis functions and integrated in order to compute the L^2 inner product, as is required in the continuous Galerkin formulation. However, since Gauss quadrature will only produce exact values for integrals of polynomials of degree $O(2P)$ at a simulation polynomial order of P , aliasing errors are introduced due to the quadratic nonlinearity present in the Navier-Stokes equations. When simulations are adequately resolved, this aliasing error usually does not affect the robustness of the simulation. However, when under-resolution is used for implicit LES, this aliasing effect leads to a significant buildup of error as the simulation progresses in time, and usually causes the simulation to abruptly diverge.

We note that the nonlinear terms of the Navier-Stokes equations are consistently integrated if the elements are straight-sided. In this case, the Jacobian of the mapping which defines the coordinates of the element is affine with constant determinant. However, where the element is curved, this mapping is an isoparametric polynomial expansion, which when incorporated into integrands, leads to an additional source of aliasing error. In this work, we do not take this source of error into account. A more detailed description of these aliasing errors, as well as means of suppressing them, can be found in [42]. Whilst it is true we could likely suppress aliasing errors using SVV, which we describe below, it would require stronger diffusion together with a lower cut-off mode, leading to reduced accuracy of the overall solution. Additionally, since the SVV operator is anisotropic, whereas dealiasing is isotropic, the two do not completely overlap. Therefore a reduced amount of regularisation can be achieved using dealiasing.

In regards to the second point, we first note that the energy spectrum of the flow consists in a resolved range of wave numbers, the large eddies, and an un-resolved range, the turbulent or dissipative scales, for higher wave numbers. Because of this cut-off the higher wavenumber dissipative scales are not resolved for LES. The energy build-up at high-wavenumber and the coupling through the nonlinear term down to lower wave numbers may lead to unstable computations at worst and erroneous energy spectra at best.

Spectral Vanishing Viscosity (SVV), first introduced by Tadmor [19] for spectral Fourier methods, aims to damp the high-wavenumber oscillations without impeding the physics of the flow at lower wavenumbers, thereby stabilising the simulation and preserving the accuracy of the solution. In this approach one adds an

additional reaction term of the form

$$\epsilon_{\text{SVV}} \frac{\partial}{\partial x} \left(\hat{Q} \star \frac{\partial u}{\partial x} \right)$$

where ϵ_{SVV} is a constant, \star denotes the convolution operator and \hat{Q} is a kernel dictating which modes receive damping. This approach was extended to the Navier-Stokes equations by Kirby & Sherwin [43], Karamanos and Karniadakis [44] and has been extensively used by Pasquetti *et al.* [45], Severac and Serre [46], Xu *et al.* [47] as well as Lamballais *et al.* [48].

We also stress that the oscillations stabilized by the SVV method are sub-element oscillations. The intrinsic nature of the spectral/*hp* element methods results in degrees of freedom within each element. When the solution field is under-resolved, it is no longer guaranteed to be smooth. This therefore leads to the development of spurious high-frequency oscillations in the polynomial representation of the solution inside each element, arising from Gibbs phenomena occurring between two connected elements. The aim of SVV stabilisation is to prevent these sub-element oscillations, since they may lead to oscillations occurring in neighbouring elements and ultimately to divergence of the computed solution.

In the context of the simulations presented here, we introduce artificial damping as an implicit sub-grid scale model through the Spectral Vanishing Viscosity (SVV). We appreciate that there may be different views of the definition of implicit LES. We have adopted the definition of Sagaut [13], who explicitly refers to SVV as an implicit LES model and states that “*using a numerical viscosity with no explicit modeling are all based implicitly on the hypothesis [...] the action of subgrid scales on the resolved scales is equivalent to a strictly dissipative action.*” The only influence of the sub-grid scales on the resolved scales is therefore dissipative.

The key point in SVV filtering is that, due to the shape of the kernel $\hat{Q}(k)$,

$$\hat{Q}(k) = \begin{cases} \exp\left(-\frac{(N-k)^2}{(M-k)^2}\right), & k > M, \\ 0, & k \leq M, \end{cases}$$

artificial viscosity for any mode number k is only applied above a cut-off mode M . For the higher modes, the total viscosity can thus be expressed as $1/Re + \epsilon_{\text{SVV}}$.

The SVV operator was incorporated into the velocity correction scheme of the incompressible Navier-Stokes equations inside Nektar++ by following the approach presented by Kirby & Sherwin [43], where the elemental Laplacian operator is convolved with the kernel \hat{Q} . The computational cost is therefore negligible since the only cost involved is during setup. However, we note that the addition of SVV can lead to higher iteration counts in the conjugate gradient method used to calculate the intermediate pressure field and perform the velocity correction. This effect can be mitigated through the use of appropriate preconditioning strategies [49].

In our SVV-iLES method the parameters do not adapt automatically to the flow (i.e. without the input of an experienced user), although methods have been proposed to overcome this constraint by implementing an adaptive SVV diffusion [44, 50]. These methods however still require the same number of parameters to be calibrated on a case-by-case basis and increase the computational runtime cost, as the matrix systems which represent the diffusion operator need to be rebuilt whenever either parameter is changed. We have therefore not considered such approaches here. Also note that we do not use spatially-variable SVV diffusion coefficient or wall functions to limit the amount of damping near solid walls.

As reference, the values of the SVV parameters used by different groups, including the simulations performed here, are reported in Table 1. Since we do not have a detailed *a priori* knowledge of the flow features and, consequently, of the sub-grid flow physics, we have chosen our SVV parameters arbitrarily so that they ensure a non-diverging solution. For other simpler cases in the literature, more effort has been made to more rigorously quantify the use of specific SVV parameters [48]. For the sake of comparison however, we report the parameters used in previous studies and stress that our choice aligns reasonably closely with that of previous studies. We recognise greater exploration is necessary for more complex cases. Research along these lines is presently being conducted by Moura *et al.* [51].

3.3 Geometry and mesh generation

The rectangular wing investigated numerically has a NACA 0012 profile, with a rounded wing cap (consequently a longer semi-span where the wing is thickest) and a blunt trailing edge. The semi-span, without the cap is, $b = 0.91[m]$ and the chord is $c = 1.22[m]$ which correspond to an aspect ratio of $A = 0.75$. The

| | M | ϵ_{SVV} |
|-----------------------|--|-------------------------|
| Tadmor[19] | $\frac{1}{3}N$ | $1/N^2$ |
| Pasquetti[45, 52, 53] | $\{\sqrt{N}, \frac{1}{3}N, \frac{1}{2}N, \frac{3}{5}N\}$ | $\{1/N, 1/4N, 4/N\}$ |
| Xu[47] | $\{N-2, \frac{2}{3}N\}$ | $1/N$ |
| Karamanos[44] | $\frac{15}{21}N$ | $1/N$ |
| Kirby[50] | $5\sqrt{N}$ | $5/8$ |
| Present study | $0.5N$ | 0.1 |

Table 1: Different values for the SVV parameters (diffusion ϵ_{SVV} and cut-off mode M) where $N = P - 1$ for a discretization of polynomials of order P .

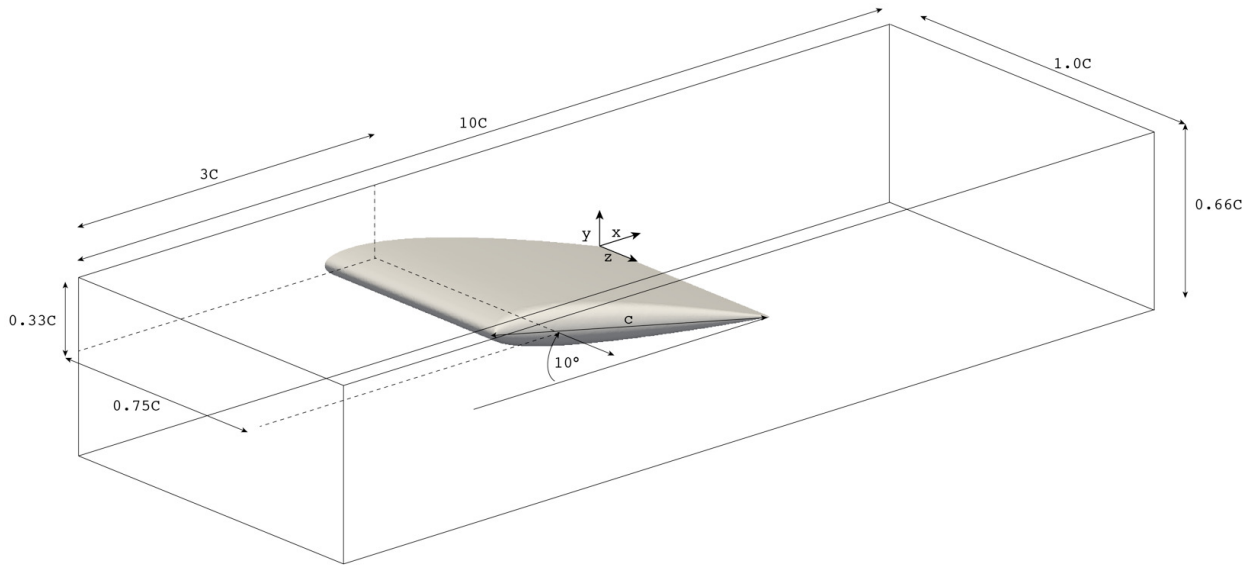


Figure 2: Computational domain representing the test section in the wind tunnel used by Chow *et al.* [1] for their experiment.

boundary layer tripping mechanism [1] used in the experiment is not reproduced in the mesh. We represent the test section of the low speed wind tunnel located in the Fluid Mechanics Laboratory of NASA Ames Research Center used by Chow *et al.* [1] for the experimental work, by a $0.66c \times c \times 10c$ cuboid domain as shown in figure 2. We do not model the wind tunnel sections upstream and downstream of the test section. A Cartesian coordinate system (x, y, z) is used to locate point within the computational domain with its origin the wingtip trailing edge, where x is aligned with the streamwise direction and y, z are the two transverse ordinates.

Regarding the interference between the primary vortex and the wind tunnel walls, Chow *et al.* decided to use as large a model as possible while still avoiding severe viscous interaction between the wall and the primary vortex through significant growth and/or separation of the boundary layers on the wind tunnel walls. The authors of the experiment warn against large inviscid effects (mirror effects) due to the close proximity of the wall that most likely influence both the primary and secondary vortices. It should also be noted that the significant blockage created by the large wing in the relatively small wind tunnel section accelerates the flow around the wing. Hence the absolute angle of attack, perceived by the wing, is around 2° higher than the angle of attack prescribed by the geometry.

Meshing methodology When considering complex geometries, even generating a linear, straight-sided mesh poses a significant challenge. We have therefore turned to commercial mesh generators, which provide a robust approach to generating linear straight-sided meshes, but generally lack support for high-order elements. We note that for high-order simulations, elements which lie on the boundary must be curved so that they align with the underlying geometry. Using straight-sided high-order elements can significantly alter the physics that form near boundaries and thus downstream of the boundary.

The commercial software we use first imports the CAD geometry, in this case the wing, and makes a fine tessellation of the surface. This tessellated surface is then used to produce the surface mesh. As we have the meshed surface and the original IGES (or CAD) geometry, but not the intermediary tessellation, we are presently unable to add the necessary curvature to the linear mesh by interrogating the CAD geometry directly. To smooth the mesh we adopt an alternative, patch-based technique known as spherigons [54] which rely on surface normals that are obtained from a fine triangulation generated by the commercial software.

The robust high-order three step mesh generation procedure used is summarized in Fig. 3 and the interested reader should refer to Moxey *et al.* [55] for further details. Our meshing procedure generates a coarse single-element boundary layer of prisms which are curved using spherigons at the wing surface, with straight-sided tetrahedra filling the rest of the volume. Each prism is split using an isoparametric method in the wall-normal direction, which allows us to achieve the desired wall normal resolution whilst preventing the self-intersection of the boundary layer elements. The tetrahedra grow from the prism layer in a controlled manner in regions of interest, such as the vortex path, where we impose a regular element size to avoid introducing additional mesh induced error.

Comparative degrees of freedom The implicit diffusion from the SVV operator preserves the convergence properties of the underlying scheme. It does not degrade the exponential rate of convergence of the accuracy of a solution achievable for a sufficiently smooth field [47]. We have focused on using our anisotropic prism refinement technique to capture the wall-normal near-wall resolution. In this region we have measured that across the wing surface, the placement of the closest grid point satisfies $y^+ < 1$. With this level of resolution, we can accurately capture the sub-viscous layer of the flow field and resolve the high shear of the boundary layer profile. However the resolution of subsequent elements is not enough to, for example, capture the extremely fine scale of the turbulent boundary layer characteristics. Additionally, for computational reasons, we clearly cannot resolve with a similar level of accuracy in the wall-tangential direction. We do appreciate that this may very well play an important role in capturing the flow in the region of the vortex roll-up. We discuss this further in the presentation of our results.

The present mesh is composed of 243,000 elements of which 24,500 are prisms around the wing surface and 218,500 are tetrahedra growing from the three prism layers to the wind tunnel walls. The prism layer represents roughly 20% of the total number of degrees of freedom. Running this computation with 5th order polynomials (i.e. 6th order accuracy in space) amounts to roughly 16.7 million degrees of freedom; around 40% fewer degrees of freedom than used by Uzun *et al.* [5] for their LES. Table 2 compares degrees of freedom for our SVV-iLES method with other studies of this case.

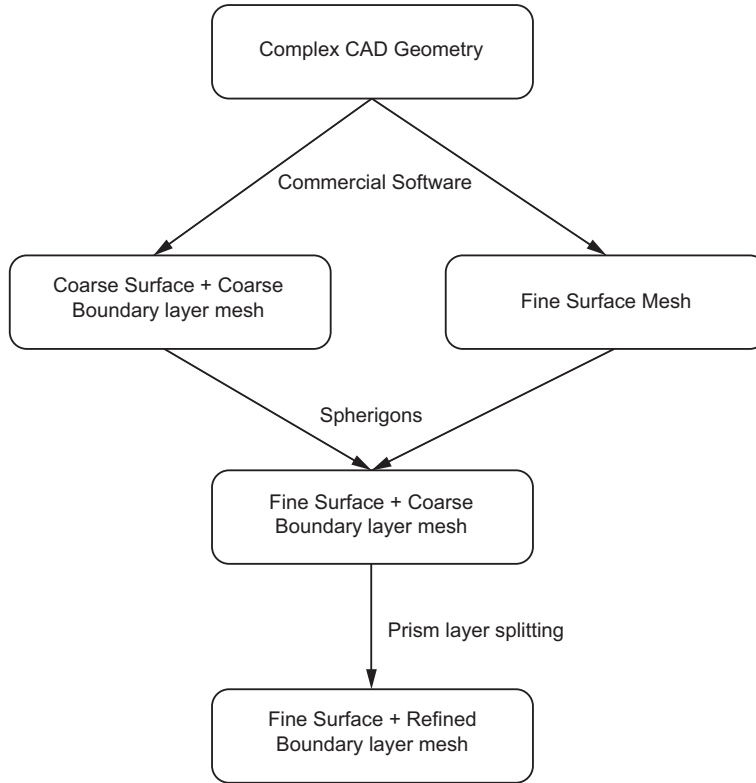


Figure 3: Robust three-step meshing procedure.

| Method | DOF ($\cdot 10^6$) |
|-----------------------------------|----------------------|
| RANS (modified Baldwin-Barth)[56] | 2.5 |
| RANS (Lag RST)[11] | 13.8 |
| LES [5] | 26.2 |
| iLES [37] | 26 |
| Present study | 16.7 |

Table 2: Comparison of mesh used by different methods, converted to degrees of freedom (DOF)

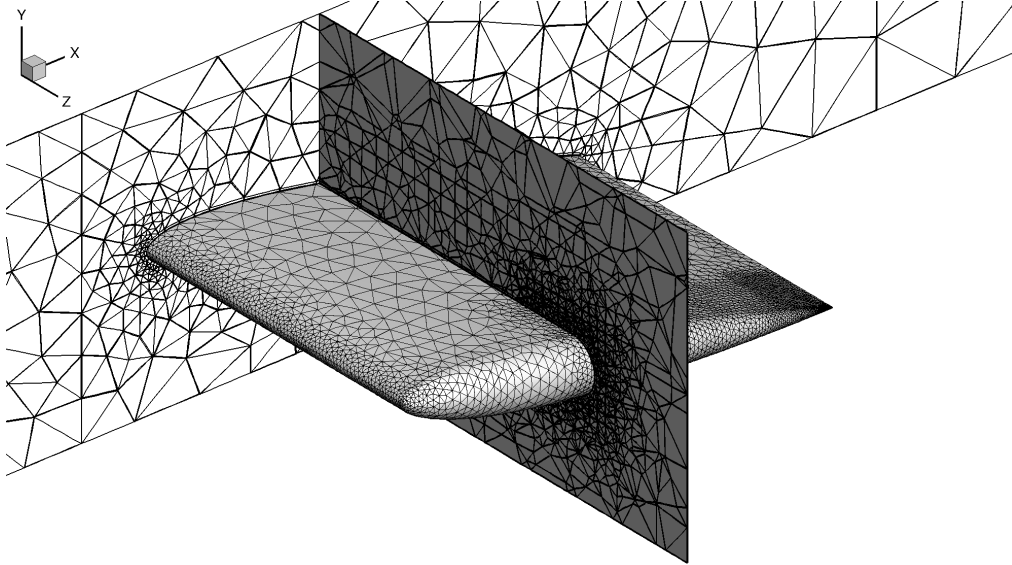


Figure 4: Overview of the coarse surface mesh and two planes, spanwise cut at the root of the wing and streamwise cut around mid chord. For sake of clarity quadrature/collocation points within each surface element are not shown here.

3.4 Initial and boundary conditions

The simulation is impulsively started from $u/U_\infty = 1$ throughout the domain, except at the no-slip boundaries where $u/U_\infty = 0$, at a low $Re_c \approx 10$. We then gradually increase the Reynolds number by a factor of 10, each time waiting for two convective time units defined as $t_c = c/U_\infty$, until the simulation reaches the desired Reynolds number. To improve computational efficiency the polynomial order P of the discretization is increased with Reynolds number, with $P = 2$ for $Re_c = 10$ and $P = 6$ for $Re_c = 1.2 \cdot 10^6$. At the outflow, we impose the boundary condition developed by Dong *et al.* [57] that balances the kinetic energy influx through the outflow boundary condition to prevent instability. The computational setup differs from the experimental setup in three ways. We discuss these and their possible influence on the results in the following paragraph.

Firstly, the boundary layers developing on the wind tunnel walls are neglected, by using a free slip condition. The primary vortex is located sufficiently far away so that the viscous interaction between the primary vortex and the wind tunnel walls is much weaker than the interaction between the primary vortex and the wing surface via the secondary structures.

As a first approximation, the wall acts, inviscidly, as a symmetry condition. Since the computed location of the vortex is similar to the experimental data, the inviscid interaction between the vortex and the wind-tunnel walls is assumed to be of similar intensity. Secondly, as with other LES studies, we do not model turbulence at inflow. As we shall see in the results section, despite the lack of a turbulent inflow we still see good comparisons against experimental data. Finally the boundary layer on the wing is not tripped. The tripping of the boundary layer near the leading edge has been reported to increase the diameter of the vortex (measured by the peak to peak distance of the vertical velocity) by 30% [29]. McAlister also report that adding a boundary layer trip changes the streamwise component of the velocity from a small excess to a large deficit at the position $x/c = 4$; however we do not observe the vortex that far downstream. The tripping of the boundary layer might affect the interaction between the primary and secondary vortices and has been reported to decrease the inboard movement of the primary vortex along the span [29].

3.5 Temporal evolution

The Navier-Stokes equations are integrated in time using a second-order accurate stiffly-stable implicit-explicit scheme [58]. The advection term is explicitly integrated, whereas the viscous term is implicitly integrated. This therefore relaxes the sometimes stringent, diffusion stability condition $\Delta t \propto \Delta x^2/\nu$. The CFL restriction $\Delta t \propto \Delta x/u$, where u is the advection velocity within each cell, remains however. Because the mesh we consider

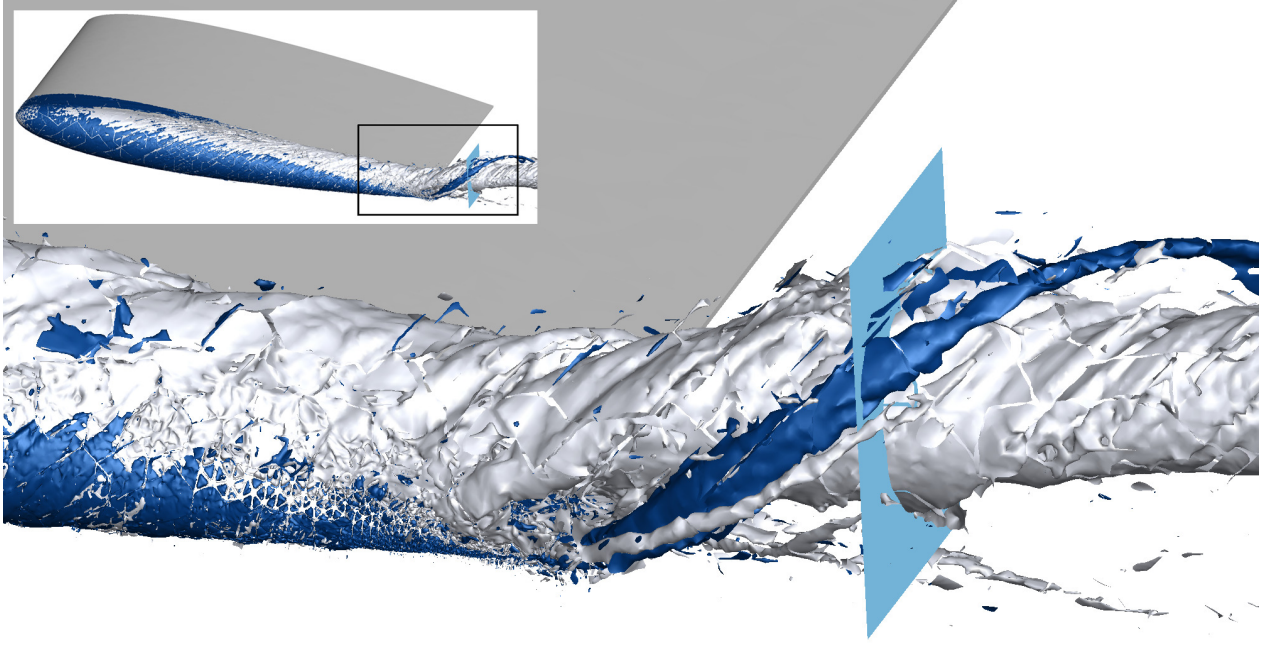


Figure 5: Contours of iso-helicity showing the interaction between the primary (in light grey) and a secondary vortex of opposite rotational sense (in blue, or dark grey). The light grey/blue plane denotes the location of the streamwise cut $x/c = 0.125$ at which results are compared with experiment in Figs. 10-11.

is coarse, we assume numerical error is dominated by error from the spatial discretization. The time step used for the computation normalized by the convective length scale of the chord t_c is $\Delta t/t_c = 1.6 \times 10^{-6}$ which translates into a maximum normalized sampling frequency of $3 \cdot 10^5$. For spectral/ hp element methods using a second order implicit-explicit time integration scheme, the analog to the CFL definition imposes a restriction on the maximum timestep of the form [40] $\Delta t < \Delta x / (\max_{\Omega^e \in \Omega} \{|V^e| P^2\})$ where we assume $\max |V^e| \sim U_\infty$. For the present mesh, where the smallest mesh element is $10^{-4}c$ and using 5th order polynomials, the timestep restriction is of the order of $10^{-5}t_c$. In practice, since the velocity in some regions can be significantly larger than U_∞ , we use a timestep one order of magnitude smaller.

4 Results and Discussion

In this section, the performance of the SVV-iLES method is evaluated by simulating the development of the wingtip vortex in the near field and comparing the results against the experimental study by Chow *et al.* [1] as well as the previous LES by Uzun *et al.* [5].

We define the *near field* to be the region above and below the wing and up to one chord length downstream of the trailing edge. In this context the *mid-field* is the region from c to $10c$ and the *far-field* is at a distance of more than $10c$ from the trailing edge. To put the challenge of accurately computing the vortex into perspective, we outline the typical tracking distances of interest for different applications. The automotive industry is interested in tracking the vortex for roughly $20c$. For wind turbines and helicopters blades, with an aspect ratio of roughly 10, the study of the interaction between the rotor blades and the preceding blades that leads to noise and structural vibration, requires tracking the wingtip vortex over more than $60c$ for one revolution. In this study an effort is made to characterize the performance of the modeling method both in the three-dimensional turbulent boundary layer and in the rollup wake. It is supposed that accurate modeling of the vortex in the near field downstream of the trailing edge pre-supposes an accurate modeling of the three-dimensional boundary layer roll-up on the wing surface.

The vortex can loosely be defined as the region in which the fluid has high helicity, low relative pressure

and an axial velocity surplus. Different methods have been developed for defining the center of a vortex, but these can prove challenging to apply in the near wake where the vortex is forming as a consequence of the shear layer roll-up. These methods include helicity peak correction, vorticity peak, Q -criterion, zero in-plane velocity and axial velocity peak. It has been shown that the helicity peak correction method is best suited for estimating the vortex core radius, axial velocity peak and swirl velocity peak. Giuni & Benard [23] assert that the centering method chosen should depend on the key aspect of interest but the robustness of these methods is not sufficient for identifying the vortex as it develops from the shear layer roll-up and interacts with secondary structures. For this reason the method of the manual location of the vortex core by identifying local pressure minima has been favored. This method has also been used by Chow *et al.* so this source of error should be taken into account when appreciating the discrepancy between reported core locations (Fig. 8) in this region.

The flow over the wingtip develops into a highly skewed three-dimensional boundary layer that rolls up and detaches into a rapidly rotating vortex, at a distance of around $0.5c$. This forms an increasingly low pressure region in the vortex core that gradually accelerates the fluid entering the core into a jet characterized by a notable normalized axial velocity surplus. This strong vortex is thought to be laminar and persistent, extending many chord lengths downstream of the trailing edge. The challenge from a modeling perspective comes from the three-dimensional boundary layer, the detachment and the strong curvature induced both by the geometry and by the many interacting vortical structures. Two key regions of the flow are used to assess the performance of the SVV-iLES method against the experimental data of Chow *et al.* [1]: the wing surface and the vortex core. These two regions are of particular interest because they radically differ in nature. Most classical turbulence models can capture turbulent boundary layers well, but few of these can accurately model the vortex core where curvature of the streamlines is high [59].

In the second region of interest, the vortex core, the key feature to reproduce is the low pressure region driving the jetting phenomena or the normalized axial velocity surplus. Inside this region, the high value of u_{\max}/U_{∞} at the trailing edge, and the low decay within the first chord length downstream of the trailing edge at $x/c = 0.867$ is a challenging feature to capture. We will therefore compare our results, as well as those from previous computations, against the reported experimental values of $u_{\max} = 1.77U_{\infty}$ and $1.59U_{\infty}$ respectively from Chow *et al.* [1]. Uzun *et al.* [5] underpredict the peak normalized and time averaged axial velocity by more than 20%, albeit at a lower chord Reynolds number $Re_c = 5 \cdot 10^5$. The $k - \omega$ based RANS computation by Churchfield *et al.* [15] report a 150% error, with respect to the experimental data by Chow *et al.* [1], in the C_p distribution within the vortex at $x/c = 0.867$. Even the $k - \omega$ SST-RC RANS [15], that predicts the C_{p_0} at $x/c = 0.867$ with less than 10% error, has nearly 20% error for the estimation of the axial velocity surplus and 30% error for the static pressure in the core at $x/c = 0.867$.

The results from SVV-iLES and evaluation with respect to experiment for the two regions of interest is presented in the next section. All results presented here have been time-averaged over three chord convective length or $1t_c$. We assume the flow is fully developed when the C_p distribution on the wing-surface at the span-wise location $z/c = 0.899$ converges to a smooth curve.

4.1 Wing Surface

4.1.1 C_p distribution

Chow *et al.* [1] reported the pressure distribution at two spanwise locations. The first cut, at $z/b = 0.833$, is situated inboard of the vortex core where its influence is mild, whereas the second is located at the vortex core in $z/b = 0.899$. At this position, the presence of the vortex leads to a distinctive pronounced suction region. The extent of this region upstream depends on the shape of the roll-up layer. The presence of the vortex reduces the pressure in this region which translates into an increase in lift.

Despite a relatively good agreement with experiment for the C_p distribution at the spanwise location $z/c = 0.833$ (Fig. 6a), at the spanwise location of the developing primary vortex (Fig. 6b), the SVV-iLES computed results under-predict the vortex suction from $x/c = 0.5$ to $x/c = 0.9$ and significantly over-predict the suction for the last $0.1c$. Coarse tangential resolution, in the first $0.5c$, may have led to a strong SVV dissipation that which in turn significantly damped the early growth of the vortex over the wing surface. The sudden change in trend at $x/c = 0.9$ might be due interaction between the primary and a secondary the secondary vortex. With this exception however, the main features of the flow are well captured.

It should be noted that the instantaneous field is noisy because of the unsteady nature of the boundary layer

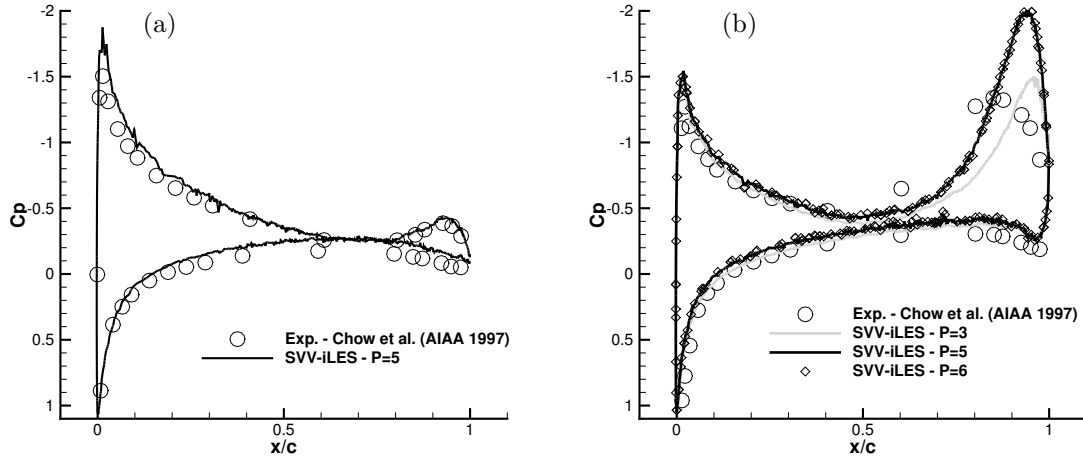


Figure 6: Comparison with experiment [1] of time-averaged C_p distribution over $3t_c$ time units as a function of streamwise position, with the leading edge in $x = 0$, at spanwise location $z/b = 0.833$ (a) and $z/b = 0.899$ in (b) where we also show the results from the uniform grid-refinement study (convergence in P). The number of mesh degrees of freedom for 4th, 6th and 7th order accurate in space are 5.7M, 16.7M and 25.3M respectively. The 50% increase in number of degrees of freedom when using 7th instead of 6th does not significantly affect the pressure distribution on the wing at the spanwise location $z/c = 0.899$.

at this high Reynolds number and is obviously reduced as we average over longer time intervals, which explains the residual noise in the C_p distribution (Fig. 6a-b). The use of the spherigon mesh smoothing technique in the representation of the geometry may also lead to some higher frequency oscillations and thus less smoothness in the distribution. Adding further diffusion from the SVV may help in removing some oscillations. However, additional diffusion might lead to an artificial reduction of the Reynolds number.

4.1.2 Resolution study

Although this test case is computationally expensive to simulate, we have performed a limited p -refinement study of the flow physics, using the C_p distribution as a benchmark for observing convergence and providing a form of self-validation. In these tests, the polynomial order was varied, comparing the $P = 5$ results that we present here to results at $P = 3$ and $P = 6$. The resulting C_p distributions, presented in figure 6b, show very little difference between the $P = 5$ and $P = 6$ cases, despite a 50% increase in the total number of degrees of freedom. However, there is a significant difference between that of $P = 3$ and $P = 5$. Whilst there is still variation between the experimental results and both $P = 5$ and $P = 6$, we can at least conclude that in terms of polynomial order the simulation is well-resolved.

We note that this type of refinement is good in that it is hierarchical and so all the degrees of freedom at lower polynomial orders are contained within the higher order simulations. It does not, however, guarantee that there cannot be regions which are still not captured and so the basic features of the flow will remain reasonably similar. Further work is therefore required to generate a larger sequence of meshes to study the effect of refinement in terms of element size. However, given the significant undertaking of this type of study and the convergence we have obtained in p , we do not consider this here and use the $P = 5$ results in the coming section.

4.2 Propagation of the vortex core in the near-wake

In the vortex core we track the normalized time-averaged axial velocity, the static pressure and at the location of the vortex both in the spanwise direction (z) and normal to the suction side direction (positive y), as shown in figures 7 and 8. Therefore both time-averaged pressure coefficient and axial velocity have not been corrected for the error stemming from possible meandering. In this section we also presents an overview of the development of the vortex in the near wake. A comparison shown for both streamlines and time-averaged

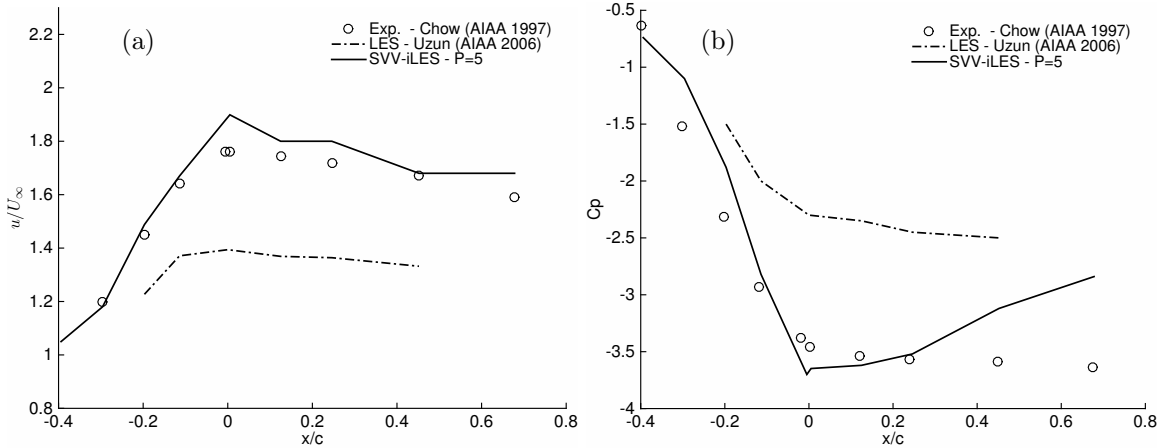


Figure 7: Comparison with experiment [1] and previous LES by Uzun *et al.* [5] of the progression of (a) axial velocity and (b) C_p distribution in the vortex core. The origin, $x/c = 0$, is taken to be the position of the wingtip trailing edge.

normalized axial velocity at two crossflow locations: over the wing towards the trailing edge at $x/c = -0.114$ and in the near wake at the $x/c = 0.125$. These results are shown in figures 9 and 10.

4.2.1 Normalized axial velocity in the vortex core.

The progression of the axial velocity of the vortex can also be affected by the presence/absence of a boundary layer trip as reported by McAlister [29]: for $Re_c = 1.5 \cdot 10^6$ a NACA 0015 profile at angle of attack $\alpha = 12^\circ$ the streamwise component of the velocity in the vortex core has a small jetting behavior ($< 5\%$ velocity excess) without the trip and a significant 20% deficit ($u/U_\infty \approx 0.8$) when a boundary layer trip is added to the leading edge. In Fig. ?? we report the streamwise progression of the normalized axial velocity. Our modeling adequately resolves the strong jetting behavior measured experimentally. We do however over-predict the peak axial velocity in the vortex core by 6% with respect to the experimental value.

4.2.2 Static pressure within the vortex core.

In Fig. ?? we report the streamwise progression of the vortex core static pressure. Despite a relative error of less than 10% over the wing surface the error grows linearly downstream of the trailing edge reaching 30%. Accurately capturing the low pressure region within the vortex core and sustaining this low pressure even just one chord distance downstream of the trailing edge is particularly challenging. The linear increase in pressure is most likely the result of either too coarse a mesh within the vortex core and/or too strong a contribution from the SVV. When the grid is too coarse to adequately capture a gradient the SVV filter damps out part of its kinetic energy. Neglecting compressibility effects, this resulting decrease in jetting velocity increases the pressure (or decreases the suction of the vortex).

4.2.3 Vertical position of the vortex core.

The vertical location of the primary vortex core is computed to be 20% lower than both the experiment and previous LES (Fig. 8a). The change in attitude as the vortex leaves the proximity of the wing surface follows a similar trend, with the core remaining at the same distance above the wing surface from streamwise location $x/c = -0.4$ from the trailing edge, to the trailing edge $x/c = 0$ and then showing a pronounced upward trend from the leading edge to the experimentally reported $x/c = 0.4$ location downstream of the leading edge. Fig. 9a shows the computed cross-section of the vertical vortex profile above the wing surface, with the same position measured experimentally (fig. 9b) and in the previous LES result of Uzun *et al.* (fig 9c). Despite a discrepancy regarding the vertical position of vortex core, we seem to be qualitatively agreeing with the experimental results. In particular, the shape of our computed vortex is closer to the isotropic round shape of the experimentally obtained vortex, particularly when compared to the previous LES result. The topology of

the flow in the region $0.03 < y/c < 0.06$, with the presence of a secondary vortex, is also qualitatively closer to the experimental results than the previous LES. We should note however that the location of the SVV-iLES computed structures is different with respect to those measured experimentally. Whilst it is difficult to explain this discrepancy without a further series of detailed simulations, one possible explanation is in the tangential grid spacing. We note that for computational reasons, this is clearly not as fine as the wall-normal direction, and this may therefore play a key role in influencing the detachment location and therefore vertical position of the vortex core. It is also interesting to remark how accurate the LES results from Uzun *et al.* are at predicting the vertical position of the vortex core above the wing despite significantly different flow topologies (Fig. 9a and Fig. 9c).

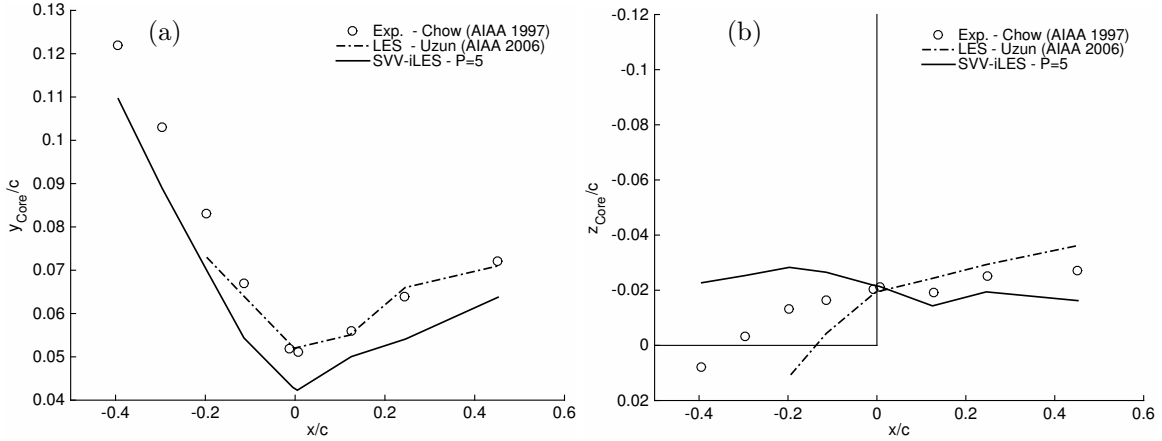


Figure 8: Comparison with experiment [1] and previous LES by Uzun *et al.* [5] of the vertical position of (a) the vortex above the wing and (b) spanwise location. The origin, $z_{core}/c = 0$ and $y_{core}/c = 0$ is taken to be the position of the wingtip trailing edge. The position of the wing is identified with the rectangle in b).

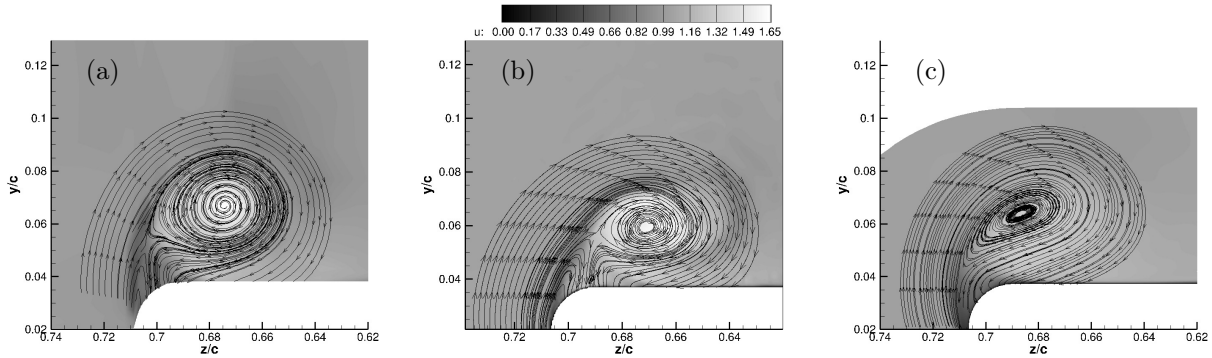


Figure 9: SVV-iLES computed streamlines and normalized time-averaged axial velocity at the crossflow plane $x/c = -0.115$ downstream of the trailing edge in b) compared against experimental results from Chow *et al.*[1], in (a) and previous LES results by by Uzun *et al.*[5], in (c).

4.2.4 Spanwise position of the vortex core.

The spanwise position of the computed vortex core is compared against both the experimental data of Chow *et al.*[1] and previous LES results by Uzun *et al.* [5]. Three key features of flow can be assessed by this figure: the location of the origin of the primary vortex, the location at the trailing edge and the evolution of the vortex as it leaves the vicinity of the surface of the wing. There is good agreement between experimental data and both LES regarding the position of the vortex at the trailing edge. There is, however, a significant discrepancy regarding the origin of the vortex. Indeed both Chow *et al.* [1] (circles in Fig. 8b) and Uzun

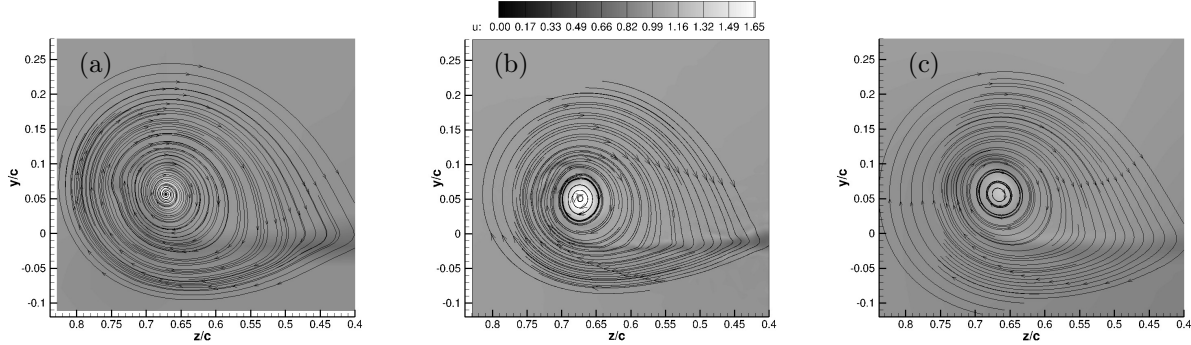


Figure 10: SVV-iLES computed streamlines and normalized time-averaged axial velocity at the crossflow plane $x/c = 0.125$ downstream of the trailing edge in b) compared against experimental results from Chow *et al.* [1], in (a) and previous LES results by by Uzun *et al.* [5], in (c). Fig. 5 acts as a companion figure to locate the $x/c = +0.125$ with respect to the primary and secondary vortices with a three dimensional perspective of the flow in this region. Fig. 11 complements Fig. 10b in aiding the identification of the secondary vortex with respect to streamlines and also the streamwise component of the vorticity.

et al. [5] (dot-dashed line in Fig. 8b) report the origin of the primary vortex in the region of the wing cap whereas the present results show the origin to be on the suction side of the wing around mid-chord. McAlister & Takahashi [29] as well as Thompson [60] reported the origin of the vortex on the suction side of a NACA 0015 profile for a similar case. McAlister & Takahashi [29] also report tripping the boundary layer decreases the inboard movement of the primary vortex along the span without altering its distance above the wing. This may offer possible insight into the difference in spanwise trajectory between Uzun’s LES computed vortex which has a more pronounced inboard movement than Chow’s experiment.

The most interesting feature of the flow that can be analysed with Fig. 8b is the evolution of the vortex as it leaves the vicinity of the surface of the wing. The experimental results of Chow *et al.* show two distinct kinks at $x/c = 0.125$ and then $x/c = 0.452$. This is particularly evident when comparing against the previous LES of Uzun *et al.*, where the progression of the vortex core moves steadily inboard. We believe these kinks are the result of the interaction between the primary vortex and a secondary vortex orbiting around it. Evidence of this secondary vortex can be seen in both the comparisons of the streamwise-normal streamlines shown in Fig. 10a with the notable presence of a flat spot in the region $0.72 < z/c < 0.75$ and $0.01 < y/c < 0.07$. Our numerical results also show a similar flat spot, albeit in slightly different position, in region $0.72 < z/c < 0.75$ and $0.06 < y/c < 0.1$. By plotting the streamwise component of the vorticity vector in this region we can correlate these flat spots to a weaker, counter rotating, secondary vortex (Fig. 11a). In Fig. 11b we enlarge this region of interest to evidence the weaker, counter rotating vortex in light grey. In these two figures the primary vortex appears in dark grey. This secondary, weaker, counter rotating vortex can also be seen when visualising the iso-helicity surfaces. In Fig. 5 the primary vortex appears in grey and the secondary vortex in dark grey (or blue if visualised in color). The light grey (light blue) surface represents the spanwise location $x/c = +0.125$ at which the comparison is made between experiment, previous LES and present results for Fig. 10-11. It is also interesting to note that the computed secondary vortex seems to be out of phase, in the streamwise direction, with respect to the experimentally computed vortex. Indeed it appears in the II quadrant whereas in the experimental results it appears in the III quadrant (when viewed as in Fig. 10-11).

5 Conclusion

The SVV-iLES workflow, developed for computing unsteady vortex-dominated flows, has been assessed by comparing numerical results with experimental data by Chow *et al.*[1] for a NACA 0012 wingtip vortex test case, at a higher Reynolds number than any LES study performed to date. Overall, the results show the potential of this method to resolve the large scale features of the flow, without the use of explicit turbulence and sub-grid scale models. The use of an implicit LES presents a notable advantage over these methods, given that only two parameters are needed to control regularization and stability of the numerics.

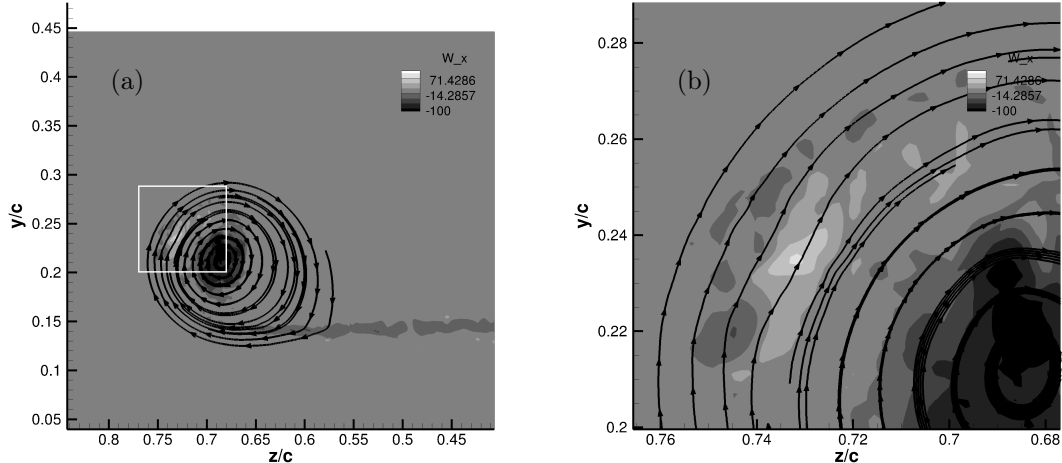


Figure 11: Streamwise component of the vorticity vector Ω_x at location $x/c = +0.125$. Both primary vortex, in dark grey, and secondary vortex in light grey in the II quadrant are visible with an overview of the flow in a) and the detail of the location of the secondary vortex in b). These figure acts as a companion to Fig. 10b.

Our results show better correlation with experimental results than previous numerical results, both in terms of the static pressure distribution, prediction of the jetting velocity, vortex spanwise location and the ability to resolve the secondary vortex interaction with the main wingtip vortex. In particular, we note that the results presented here show a good agreement in the roll-up region where both the static pressure and velocity magnitude agree within 10% of experiment. We also observe that although the mesh used in this study is coarser than ones reported in other studies, as highlighted in Tab. 2, and the Reynolds number is larger than previous investigations, the results of this study demonstrate that the SVV-iLES method can still accurately capture the essential features of the flow. However we do note that unsteady simulation obviously requires significantly more compute resource as compared to steady RANS simulations. We additionally obtain a qualitatively good agreement of the modeling of the vortex roll-up, and predict the secondary vortex and its interaction with the primary vortex over the wingtip. We believe this can be attributed both to the lower diffusion and dispersion properties of the spectral/ hp element method and to the use of an isoparametric refinement technique which provides adequate wall-normal resolution in the sub-viscous layer of the boundary region.

There are however some clear differences between the results presented here and experimental data. It is clear that the suction peak on the wing appears further downstream ($x/c = 0.95$ instead of the experimental value of $x/c = 0.85$). There is also a visible difference in the location of the secondary vortex at location $x/c = 0.867$ downstream of the trailing edge. These points seem to indicate that despite successfully modeling the secondary vortex, the interaction between the primary and secondary vortex is not yet accurate enough to reproduce experimental results. The p -refinement study presented here shows that, whilst our results are well-resolved in terms of the polynomial space, a small increase in polynomial order does not generally lead to a better correlation with the experimental data. This is likely due an under-resolution of the wall-tangential directions across of the surface of the wing and in particular in the first $0.5c$, where the primary vortex originates. Therefore, whilst a large increase in polynomial order would hopefully yield a better correlation with the experimental results, a more efficient approach to achieve convergence is likely to be a combination of both mesh and p -refinement. It is therefore clear that, together with improving the smoothness of the surface mesh and a further increase in Reynolds number to match the experiment, future studies should include additional local refinement in terms of element size in order to hopefully attain a closer agreement with the experimental results.

In summary, the SVV-iLES method has been shown to be a compelling alternative for computing complex unsteady vortex dominated flows, such as the wingtip vortex, motivating its use for complex industrially relevant cases where high-fidelity computational fluid dynamics can become an enabling technology.

Acknowledgments

The authors would like to thank Dr. Ali Uzun for sharing both experimental and LES results for figures 13-18. We also thank the reviewers of this manuscript for a number of helpful suggestions. The authors acknowledge support from the United Kingdom Turbulence Consortium (UKTC) under grant EP/L000261/1 as well as from the Engineering and Physical Sciences Research Council (EPSRC) for access to ARCHER UK National Supercomputing Service (<http://www.archer.ac.uk>). DM acknowledges supported by the Laminar Flow Control Centre funded by Airbus/EADS and EPSRC under grant EP/I037946. SJS additionally acknowledges Royal Academy of Engineering support under their research chair scheme. We also acknowledge the support from the Imperial College London High Performance Computing facilities.

References

- [1] J.S. Chow, G. Zilliac, and P. Bradshaw. Mean and turbulence measurements in the near field of a wingtip vortex. *AIAA Journal*, 35(10):1561–1567, 1997.
- [2] William J. Devenport, Michael C. Rife, Stergios I. Liapis, and Gordon J. Follin. The structure and development of a wing-tip vortex. *Journal of Fluid Mechanics*, 312:67–106, 4 1996.
- [3] L. Jacquin, D. Fabre, P. Geffroy, and E. Coustols. *The properties of a transport aircraft wake in the extended near field - An experimental study*. American Institute of Aeronautics and Astronautics, 2001.
- [4] A Heyes, R Jones, and D Smith. Wandering of wingtip vortices. In *12th International symposium on application of laser techniques to fluid mechanics*, 2004.
- [5] Ali Uzun, M. Yousuff Hussaini, and Craig L. Streett. Large-eddy simulation of a wing tip vortex on overset grids. *AIAA Journal*, 44(6):1229–1242, 2006.
- [6] Ali Uzun and M. Yousuff Hussaini. Simulations of vortex formation around a blunt wing tip. *AIAA Journal*, 48(6):1221–1234, 2010.
- [7] Vernon J. Rossow. Lift-generated vortex wakes of subsonic transport aircraft. *Progress in Aerospace Sciences*, 35(6):507 – 660, 1999.
- [8] Reza Ghias, Rajat Mittal, Haibo Dong, and Thomas Lund. *Study of Tip-Vortex Formation Using Large-Eddy Simulation*. American Institute of Aeronautics and Astronautics, 2005.
- [9] Jennifer Dacles-Mariani, Gregory G. Zilliac, Jim S. Chow, and Peter Bradshaw. Numerical/experimental study of a wingtip vortex in the near field. *AIAA Journal*, 33(9):1561–1568, 1995.
- [10] Philippe R. Spalart. Airplane trailing vortices. *Annual Review of Fluid Mechanics*, 30(1):107–138, 1998.
- [11] Matthew J. Churchfield and Gregory A. Blaisdell. Reynolds stress relaxation turbulence modeling applied to a wingtip vortex flow. *AIAA Journal*, 51(11):2643–2655, 2013.
- [12] Rajani Satti, Yanbing Li, Richard Shock, and Swen Noelting. Unsteady flow analysis of a multi-element airfoil using lattice boltzmann method. *AIAA Journal*, 50(9):1805–1816, 2012.
- [13] Pierre Sagaut. *Large Eddy Simulation for Incompressible Flows*. Springer Berlin Heidelberg, 2001.
- [14] A. Bolis, C. D. Cantwell, R. M. Kirby, and S. J. Sherwin. From h to p efficiently: optimal implementation strategies for explicit time-dependent problems using the spectral/hp element method. *International Journal for Numerical Methods in Fluids*, 75(8):591–607, 2014.
- [15] Matthew Churchfield and Gregory Blaisdell. *A Reynolds Stress Relaxation Turbulence Model Applied to A Wingtip Vortex Flow*. American Institute of Aeronautics and Astronautics, 2011.
- [16] Jennifer Dacles-Mariani, Dochan Kwak, and Gregory Zilliac. *Accuracy assessment of a wingtip vortex flowfield in the near-field region*. American Institute of Aeronautics and Astronautics, 1996.

- [17] Karthikeyan Duraisamy and James D. Baeder. Numerical simulation of the effects of spanwise blowing on wing-tip vortex formation and evolution. *Journal of Aircraft*, 43(4):996–1006, 2006.
- [18] Rajani Satti, Yanbing Li, Richard Shock, and Brad Duncan. *Computational Analysis of a Wingtip Vortex in the Near-Field using LBM-VLES Approach*. American Institute of Aeronautics and Astronautics, 2011.
- [19] Eitan Tadmor. Convergence of spectral methods for nonlinear conservation laws. *SIAM Journal on Numerical Analysis*, 26(1):30–44, 02 1989.
- [20] S. I. Green and A. J. Acosta. Unsteady flow in trailing vortices. *Journal of Fluid Mechanics*, 227:107–134, 6 1991.
- [21] M. Giuni. *Formation and early development of wingtip vortices*. PhD thesis, University of Glasgow, 2013.
- [22] Michea Giuni and Richard B. Green. Vortex formation on squared and rounded tip. *Aerospace Science and Technology*, 29(1):191–199, 8 2013.
- [23] Michea Giuni and Emmanuel Benard. *Analytical/Experimental Comparison of the Axial Velocity in Trailing Vortices*. American Institute of Aeronautics and Astronautics, 2011.
- [24] David Fabre and Laurent Jacquin. Stability of a four-vortex aircraft wake model. *Physics of Fluids (1994-present)*, 12(10):2438–2443, 2000.
- [25] D. Fabre, L. Jacquin, and A. Loof. Optimal perturbations in a four-vortex aircraft wake in counter-rotating configuration. *Journal of Fluid Mechanics*, 451:319–328, 1 2002.
- [26] L. Dieterle, K. Ehrenfried, R. Stuff, G. Schneider, P. Coton, J.C. Monnier, and J.F. Lozier. Quantitative flow field measurements in a catapult facility using particle image velocimetry. In *Instrumentation in Aerospace Simulation Facilities, 1999. ICIASF 99. 18th International Congress on*, pages 1/1–110, 1999.
- [27] L.R. Zuhail. *Formation and Near-field Dynamics of a Wingtip Vortex*. PhD thesis, California Institute of Technology, 2001.
- [28] Lavi Zuhail and Morteza Gharib. *Near field dynamics of wing tip vortices*. American Institute of Aeronautics and Astronautics, 2001.
- [29] K. W. McAlister and R. K. Takahashi. Avscom technical report 91-a-003 naca 0015 wing pressure and trailing vortex measurements. Technical report, Nasa Technical Paper 3151, 1991.
- [30] Matthew J. Churchfield and Gregory A. Blaisdell. Numerical simulations of a wingtip vortex in the near field. *Journal of Aircraft*, 46(1):230–243, 2009.
- [31] J. Dacles-Mariani, S. Rogers, D. Kwak, G. Zilliac, and J. Chow. *A computational study of wingtip vortex flowfield*. American Institute of Aeronautics and Astronautics, 1993.
- [32] T.J. Craft, A.V. Gerasimov, B.E. Launder, and C.M.E. Robinson. A computational study of the near-field generation and decay of wingtip vortices. *International Journal of Heat and Fluid Flow*, 27(4):684 – 695, 2006. Special Issue of The Fourth International Symposium on Turbulence and Shear Flow Phenomena - 2005 Special Issue of The Fourth International Symposium on Turbulence and Shear Flow Phenomena - 2005.
- [33] G. Iaccarino K. Duraisamy. Curvature correction and application of the $v_2 \hat{\Delta}^2 f$ turbulence model to tip vortex flows. Technical report, Center for Turbulence Research - Annual Research Briefs, Stanford, CA, 2005.
- [34] Matthew Churchfield and Gregory Blaisdell. *The Lag RST Turbulence Model Applied to a Vortex Flow*. American Institute of Aeronautics and Astronautics, 2008.
- [35] Matthew J. Churchfield and Gregory A. Blaisdell. Numerical simulations of a wingtip vortex in the near field. *Journal of Aircraft*, 46(1):230–243, 2009.

- [36] Oliver Fleig, Makoto Iida, and Chuichi Arakawa. Wind turbine blade tip flow and noise prediction by large-eddy simulation. *Journal of Solar Energy Engineering*, 126(4):1017–1024, 11 2004.
- [37] Li Jiang, Jiangang Cai, and Chaoqun Liu. Large-eddy simulation of wing tip vortex in the near field. *International Journal of Computational Fluid Dynamics*, 22(5):289–330, 2008.
- [38] F. R. Menter. Two-equation eddy-viscosity turbulence models for engineering applications. *AIAA Journal*, 32(8):1598–1605, 2015/07/18 1994.
- [39] C. D. Cantwell, D. Moxey, A. Comerford, A. Bolis, G. Rocco, G. Mengaldo, D. de Grazia, S. Yakovlev, J.-E. W. Lombard, D. Ekelschot, B. Jordi, Y. Mohamied, C. Eskilsson, B. Nelson, P. Vos, C. Biotto, R. M. Kirby, and S. J. Sherwin. Nektar++: An open-source spectral/hp element framework. Accepted for publication in *Computer Physics Communications*. 2014.
- [40] G. Karniadakis and S. Sherwin. *Spectral/hp Element Methods for Computational Fluid Dynamics*. Oxford University Press, second edition, 2005.
- [41] G. Karniadakis, M. Israeli, and S. Orszag. High-order splitting methods for incompressible navier-stokes equations. *J. Comp. Phys*, 97:414–443, 1991.
- [42] G. Mengaldo, D. De Grazia, D. Moxey, P.E. Vincent, and S.J. Sherwin. Dealiasing techniques for high-order spectral element methods on regular and irregular grids. *Journal of Computational Physics*, 2014.
- [43] Robert M. Kirby and Spencer J. Sherwin. Stabilisation of spectral/hp element methods through spectral vanishing viscosity: Application to fluid mechanics modelling. *Computer Methods in Applied Mechanics and Engineering*, 195(23–24):3128 – 3144, 2006. Incompressible {CFD}.
- [44] G.-S. Karamanos and G. E. Karniadakis. A spectral vanishing viscosity method for large-eddy simulations. *J. Comput. Phys.*, 163(1):22–50, September 2000.
- [45] R. Pasquetti. Spectral vanishing viscosity method for les: sensitivity to the svv control parameters. *Journal of Turbulence*, 6, 2005.
- [46] E. Severac and E. Serre. A spectral vanishing viscosity for the les of turbulent flows within rotating cavities. *J. Comput. Phys.*, 226(2):1234–1255, October 2007.
- [47] Chuanju Xu. Stabilization methods for spectral element computations of incompressible flows. *Journal of Scientific Computing*, 27(1-3):495–505, 2006.
- [48] Eric Lamballais, Véronique Fortuné, and Sylvain Laizet. Straightforward high-order numerical dissipation via the viscous term for direct and large eddy simulation. *Journal of Computational Physics*, 230(9):3270 – 3275, 2011.
- [49] S.J. Sherwin and M. Casarin. Low-energy basis preconditioning for elliptic substructured solvers based on unstructured spectral/hp element discretization. *J. Comp. Phys*, 171:394–417, 2001.
- [50] Robert M. Kirby and George Em Karniadakis. Coarse resolution turbulence simulations with spectral vanishing viscosity—large-eddy simulations (svv-les). *Journal of Fluids Engineering*, 124(4):886–891, 12 2002.
- [51] R.C. Moura, S.J. Sherwin, and J. Peiró. Linear dispersion-diffusion analysis and its application to under-resolved turbulence simulations using discontinuous galerkin spectral/hp methods. *Journal of Computational Physics*, 2015.
- [52] Richard Pasquetti. Spectral vanishing viscosity method for large-eddy simulation of turbulent flows. *Journal of Scientific Computing*, 27(1-3):365–375, 2006.
- [53] R. Pasquetti, E. Séverac, E. Serre, P. Bontoux, and M. Schäfer. From stratified wakes to rotor–stator flows by an svv–les method. *Theoretical and Computational Fluid Dynamics*, 22(3-4):261–273, 2008.

- [54] Pascal Volino and N Magenat Thalmann. The spherigon: a simple polygon patch for smoothing quickly your polygonal meshes. In *Computer Animation 98. Proceedings*, pages 72–78. IEEE, 1998.
- [55] D. Moxey, M. Hazan, J. Peiró, and S. J. Sherwin. An isoparametric approach to high-order curvilinear boundary-layer meshing. to appear in *Comput. Meth. Appl. Mech. Eng.*, sep 2014.
- [56] Jennifer Dacles-Mariani, Mohamed Hafez, and Dochan Kwak. *Prediction of wake-vortex flow in the near- and intermediate-fields behind wings*. American Institute of Aeronautics and Astronautics, 1997.
- [57] S. Dong, G.E. Karniadakis, and C. Chrysosostomidis. A robust and accurate outflow boundary condition for incompressible flow simulations on severely-truncated unbounded domains. *Journal of Computational Physics*, 261(0):83 – 105, 2014.
- [58] G. E. Karniadakis, M. Israeli, and Orszag S. A. High-order splitting methods for the incompressible navier-stokes equations. *Journal of Computational Physics*, 97(2):414 – 443, 1991.
- [59] P. Bradshaw. Effects of streamline curvature on turbulent flow. Technical report, AGARD-AG-169, 1973.
- [60] D.H. Thompson. Aerodynamics note 421 : A flow visualization study of tip vortex formation. Technical report, Defence Science and Technology Organisation Aeronautical Research Laboratories, Melbourne Australia, 1983.